Spatial clustering of microscopic dynamics governs the slip avalanche of sheared granular materials

Jiangzhou Mei [a,b], Gang Ma [a,b,*], Longwen Tang [c], Ke Gao [d], Wanda Cao [a,b], Wei Zhou [a,b]

[a] *State Key Laboratory of Water Resources and Hydropower Engineering Science, Wuhan University, Wuhan 430072, PR. China*
[b] *Institute of Water Engineering Sciences, Wuhan University, Wuhan 430072, PR. China*
[c] *Department of Civil and Environmental Engineering, University of California, Los Angeles, California 90095, USA*
[d] *Department of Earth and Space Sciences, Southern University of Science and Technology, Shenzhen 518055, Guangdong, PR. China*

ARTICLE INFO

ABSTRACT

Establishing quantifiable links between individual-particle dynamics and macroscopic response of granular materials has been a longstanding challenge, with implications in material science, geology and industry. Despite sustained efforts in uncovering generic features in both macroscopic flow and microscopic dynamics, further advance on the subject matter demands quantitative correlations to be established. We propose a 3D convolution neural network (CNN) to quantify the link between microscopic dynamics and macroscopic stress fluctuations, including both stress recharge (stick regime) and stress drop (slip regime). Through the model interpretation, microscopic dynamics is found to demonstrate distinctive spatial patterns in the stick and slip regimes, which root in the result of free volume-induced structural rearrangements and contact network dynamics, respectively. We conclude that the spatial clustering of microscopic dynamics governs the occurrence of slip avalanches and acts as the "fingerprint" of macroscopic stress fluctuation. The data-driven framework developed in this paper can be readily extended to other amorphous solids for building cross-scale relations, paving a new way to understand the complex behavior of amorphous solids.

1. Introduction

Amorphous solids, including granular materials, mental glasses and foams, are ubiquitous in our daily life, with important implications from geomechanics (Lherminier et al., 2019; Sun et al., 2018) to industry (Cheng et al., 2019) and material science (Aime et al., 2018; Y. Y. Wang et al., 2020). When stimulated by external loads, these materials may display highly heterogeneous behaviors, showing localized, irreversible rearrangements while the rest of the material acting largely as an elastic "solid" (Tong et al., 2016; Y. Y. Wang et al., 2020). The localized rearrangements, widely termed as shear transformation zones (STZs) (Falk and Langer, 1998; Jiang et al., 2020) or micro slip lines (Kosiba et al., 2019), are found spatially correlated (Cubuk et al., 2017). Note that the microscopic slip lines, demonstrating the particle-scale and short-lived shear patterns, are frequently observed before the formation of a macroscopic persistent shear band under deviatoric loads, and the nature of these structures and their relationship with the final shear bands is still a matter of much debate (Darve et al., 2021; Liu et al., 2022; Zhou et al., 2021). Moreover, a local rearrangement event may trigger other

---

* Corresponding author.
  E-mail address: magang630@whu.edu.cn (G. Ma).

nearby rearrangements and the accumulation of these rearrangements may give rise to a global avalanche (Cao et al., 2019). The different events may develop in a sequential manner at different rates. Consequently, the macroscopic response of such microscopic behavior is characterized by a series of slip avalanches alternating slow elastic loading and rapid sliding (Houdoux et al., 2021; Tong et al., 2016).

The slip avalanche phenomenon, characterized by the stress increase during the stick regime and stress softening during the slip one, is frequently studied over amorphous solids, such as granular materials (Denisov et al., 2016; Murphy et al., 2019) and metal glasses (Cao et al., 2018a; Tong et al., 2016). Specifically, the statistical features of stress fluctuations have been well described by power-law statistics, the exponent of which is influenced by many controlling factors, such as the particle shape (Murphy et al., 2019), particle breakage (Wang et al., 2021a), size polydispersity (Ma et al., 2020), confining pressure (Gao et al., 2020), etc. Over the years, a variety of analytical methods, including the mean field theories (MFT) (Dahmen et al., 2011; Ridout et al., 2022) and STZs theories (Falk and Langer, 1998; Van Loock et al., 2021), have been proposed to successfully link the statistical features of slip avalanches and transient strain-banding instabilities to internal processes. Despite all these developments, there is still no consensus on how these stress fluctuations originate from the microscopic scale and how to quantitatively link microscopic and macroscopic aspects of slip avalanches, which are crucial to obtaining a better understanding of the intermittent dynamic behavior of granular materials and the occurrence of many natural disasters, such as earthquakes and landslides.

Microscopic dynamics was recently found to be closely correlated with the magnitude of slip avalanche, where large slip events are accompanied by a series of connected STZs spanning the entire system while STZs with low concentrations are spatially dispersed during small slip events (Cao et al., 2018a; Wu et al., 2015). For the sake of clarity, it is emphasized that microscopic scale refers hereafter to the individual particle scale and macroscopic scale to the whole assembly scale. However, no quantitative relations have been established between microscopic dynamics and slip avalanches. This is essentially a longstanding puzzle among amorphous solids about how to quantitatively connect microscopic (particle-scale) dynamics to the macroscopic (system-size) behaviors (Guo and Zhao, 2016; Papadopoulos et al., 2018; Qu et al., 2021; Wautier et al., 2019). Although many upscaling models, such as the stress-force-fabric (SFF) model (Ouadfel and Rothenburg, 2001; Zhu et al., 2016b), mesoscopic mechanical models (Wautier et al., 2018; Xiong et al., 2017), nonlocal rheology model (Henann and Kamrin, 2014; Kim and Kamrin, 2020), and the FEM-DEM hierarchical multiscale framework (Guo and Zhao, 2014), are proposed for predicting macroscopic responses from the local properties, they are realized via some homogenization operations, which may lose detailed information at the particle scale. Thus, these methods are unable to reveal how the particle-scale dynamics influence macroscopic responses and how they are induced by microscopic processes, which are fundamental questions regarding the multiscale behaviors in granular materials.

Fortunately, machine learning (ML), especially deep learning (DL), offers data-driven approaches to automatically investigate the underlying relations between variables and facilitates the process of revealing complex and inexplicit patterns of large datasets. Over the past years, ML has been widely used in the communities of engineering and material science over the past years (Anantrasirichai et al., 2019; Boattini et al., 2020; Lai and Chen, 2019; McBeck et al., 2020). Particular attention has been paid to modeling the constitutive relationship of amorphous solids via data-driven approaches (Bahmani and Sun, 2022; Guan et al., 2022; Karapiperis et al., 2021; Qu et al., 2021; Wang and Sun, 2018), which has undoubtedly advanced our understandings of the mechanical behaviors and constitutive modeling of granular materials. These data-driven models are experts in predicting the general trends of stress-strain curves, whereas the predicted stress curves are actually "smoothed" and contain almost no fluctuation. In other words, they can't reproduce the slip avalanche phenomenon. Thus, we are handling a different issue compared to previous studies on predicting the whole stress-strain curves. Building an accurate multiscale relationship demands an efficient upscaling approach to consider the dynamic information of every single particle and their spatial correlation. This can't be achieved by just defining several internal
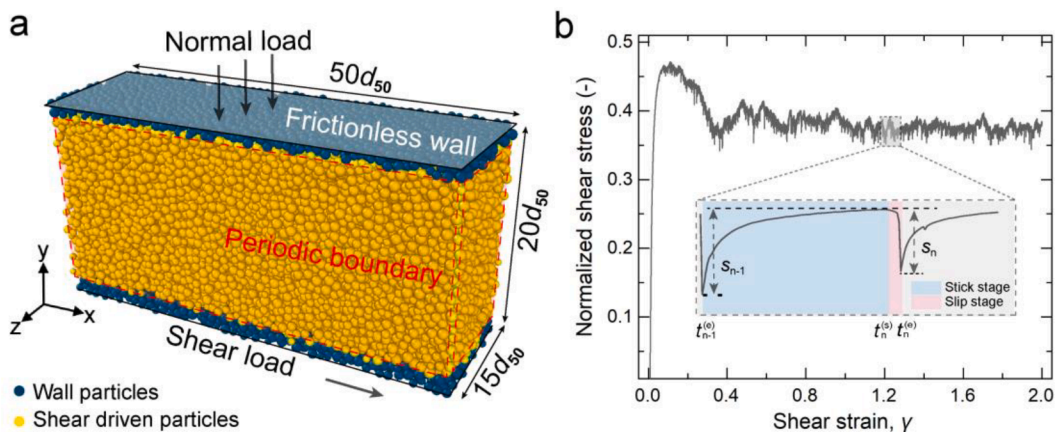
Fig. 1. DEM simulation of simple shear tests. **(a)** Schematic of the DEM model. Normal pressure and shear displacement are respectively applied on the top and bottom particle walls. Periodic boundary conditions are applied in the shear and depth directions. **(b)** Stress-strain curve resulted from the DEM simulation. The y axis denotes the shear stress σ normalized by the normal pressure p. The inset shows an enlarged stick-slip cycle which consists of stress recovery and slip stage represented by the blue and red shaded regions, respectively.

variables.

To achieve a better understanding of the relation between particle-scale dynamics and the macroscopic response of granular packing, we propose a 3D convolution neural network (3D CNN) framework, a typical form of DL, to quantitively link microscopic dynamics and macroscopic stress fluctuations, including both stress recharge (stick regime) and stress drop (slip regime). We unveil that the microscopic dynamics demonstrates different spatial patterns in the stick and slip regimes. A further model interpretation confirms that the spatial pattern of microscopic dynamics acts as the "fingerprint" of macroscopic response. Finally, we show that the spatial patterns of microscopic dynamics over stick and slip stages are the result of free volume-induced structural rearrangements and contact network dynamics, respectively. The data-driven framework develop in this paper can be readily extended to other amorphous solids for building micro-macroscopic relations, paving new ways to further understandings on the complex behavior of amorphous solids.

2. Materials and methods

2.1. Numerical simulations

In this paper, the Discrete Element Method (DEM) is utilized to obtain data of microscopic dynamics and macroscopic stress fluctuations during the stick-slip cycles of the granular system. Fig. 1a shows the simple shear model setup of the granular packing, which consists of 20,215 particles with diameters uniformly distributed from $0.8\overline{d}$ to $1.2\overline{d}$, where the average particle diameter $\overline{d} = 1.0$ mm. The particles have a density of 2900 kg/m^3, Poisson's ratio of 0.25, Young's modulus of 65 GPa, friction coefficient of 0.5, and restitution coefficient of 0.87. The size of the granular packing is set to $50\overline{d}$ (length) $\times$ $15\overline{d}$ (depth) $\times$ $20\overline{d}$ (height). We use the Hertz-Mindlin contact model to simulate the interactions between particles. The granular packing is confined by two rough particle walls for applying shear loading and normal pressure. The top wall is fixed in the shear direction, while the normal pressure is maintained constant at 10 MPa. The granular packing is sheared by moving the bottom wall in the x direction with a constant velocity while the vertical movement is constrained. The shear rate $\dot{\gamma}$, defined as the ratio of shear velocity to the undeformed sample height, is set to 0.1 to achieve stick-slip dynamics. The parameters of our simulation are consistent with many previous studies (Dorostkar et al., 2017; Ma et al., 2020). Following previous studies (Guo and Zhao, 2014; Meier et al., 2008), we have measured the minimum size of representative volume element (RVE) to be about the length scale of $8\overline{d}$. Moreover, the number of particles in our granular system is larger than many previous studies on slip avalanches, which usually contain 8000~13,000 particles (Ma et al., 2020; van den Ende and Niemeijer, 2018; Wang et al., 2021a; Zheng et al., 2021), ensuring that our granular system is much larger than the minimum representative volume element.

As shown in Fig. 1b, when sheared into the steady-state regime, the granular assembly is found to undergo typical intermittent dynamics and serrated plastic flow. The resulting stress-strain curve consists of repetitive cycles of continuous stress recoveries followed by sharp stress drops, termed respectively as stick stages and slip stages in the enlarged view of Fig. 1b. Here we normalize the resulted shear stress with the normal pressure on the top granular wall and obtain the normalized shear stress (without any unit). We then define stress fluctuation as the change of normalized shear stress at the start and end of the stick/slip stages. Thus, the stress fluctuation of a slip stage is positive, and the stick stage negative. Only the magnitudes of stress fluctuation greater than a threshold of 10^{-5} are considered. During the shearing process, we have recorded a total of 4232 stick-slip cycles.

2.2. Microscopic dynamics

Unlike crystal materials where plastic activities are mediated by well-defined topological defects termed dislocations (Salmenjoki et al., 2018), a significantly different scenario exists in amorphous solids like granular materials. Due to their disordered nature, granular materials undergo the macroscopic plastic deformation with localized particle rearrangements, demonstrating the typical dynamic heterogeneity (Y. Cao et al., 2018; Dauchot et al., 2005). Particles experience significantly different magnitudes of microscopic dynamics due to the varying environments, which can be quantified by the squared nonaffine displacement $D^2_{\min}$. Specifically, $D^2_{\min}$ measures the mean-square difference between the actual displacements of the neighboring particles relative to the central one and the relative displacements they would have if they were in a region of uniform deformation described by a locally affine tensor $\mathbf{\Gamma}$. Thus, given a system-scale strain increment $\Delta\gamma$, the corresponding $D^2_{\min}$ of the designated particle i can be calculated as

$$D^2_{\min}(\gamma, \Delta\gamma) = \frac{1}{N_i} \sum_{j}^{N_i} \left\{ \mathbf{r}_j(\gamma) - \mathbf{r}_i(\gamma) - \mathbf{\Gamma} \left[\mathbf{r}_j(\gamma - \Delta\gamma) - \mathbf{r}_i(\gamma - \Delta\gamma) \right] \right\}^2 \qquad (1)$$

where γ denotes the macroscopic shear strain of a given time, N_i is the number of the neighbors of particle i, and the subscript j iterate over the neighbors of particle i. $\mathbf{r}_i(\gamma)$ and $\mathbf{r}_j(\gamma)$ refer to the coordinates of particle i and j at a given strain γ. The locally best-fit affine tensor $\mathbf{\Gamma}$ can be obtained by minimizing the quantity $D^2_{\min}$ as (Falk and Langer, 1998)

$$\mathbf{X} = \sum_{j}^{N_i} \left[\mathbf{r}_j(\gamma) - \mathbf{r}_i(\gamma) \right] \otimes \left[\mathbf{r}_j(\gamma - \Delta\gamma) - \mathbf{r}_i(\gamma - \Delta\gamma) \right] \qquad (2)$$

$$\mathbf{Y} = \sum_{j}^{N_i} \left[\mathbf{r}_j(\gamma) - \mathbf{r}_i(\gamma) \right] \otimes \left[\mathbf{r}_j(\gamma - \Delta\gamma) - \mathbf{r}_i(\gamma - \Delta\gamma) \right] \tag{3}$$

$$\mathbf{\Gamma} = \mathbf{X} \cdot \mathbf{Y}^{-1} \tag{4}$$

In this work, particles within a cutoff distance L_c to the center of particle i are defined as its neighbors. Previous studies have indicated that a local particle rearrangement mainly causes cooperative rearrangements within its first to second neighbor shell (Y. Cao et al., 2018; Zhang et al., 2020). A larger cutoff distance will result in a more average nonaffine displacement field, and thus hampers the characterization of the heterogeneous dynamic behavior. In this context, a small cutoff distance like $2\bar{d}$ is commonly used in many previous studies for calculating nonaffine displacements (Boattini et al., 2020; Liu et al., 2021; Wang et al., 2020a), and we set the cutoff distance as $L_c = 2\bar{d}$ in this manuscript.

Moreover, previous study indicates that particles with larger nonaffine displacements are more likely to be involved in more intense plastic activities (Y. Cao et al., 2018), which enables D_{min}^2 to be employed as an indicator for the microscopic plasticity, and has been frequently used for investigating the plastic behaviors of amorphous solids, e.g. granular materials (Y. Cao et al., 2018; Cubuk et al., 2017; Zhai et al., 2022), metallic glasses (Cao et al., 2019; Wang and Jain, 2019), and colloidal systems (Ghosh et al., 2017; Liu et al., 2021). Over the past years, combing the nonaffine displacement and the machine learning approaches provokes an explosive growth of researches in unveiling the relationship the microscopic structure and microscopic plasticity (Cubuk et al., 2017; Liu et al., 2021; Wang and Jain, 2019), which has largely advancing our understanding of the nature of microscopic plasticity in amorphous solids. These studies often treat particles with nonaffine displacements larger than a given threshold as involved in the microscopic plastic events.
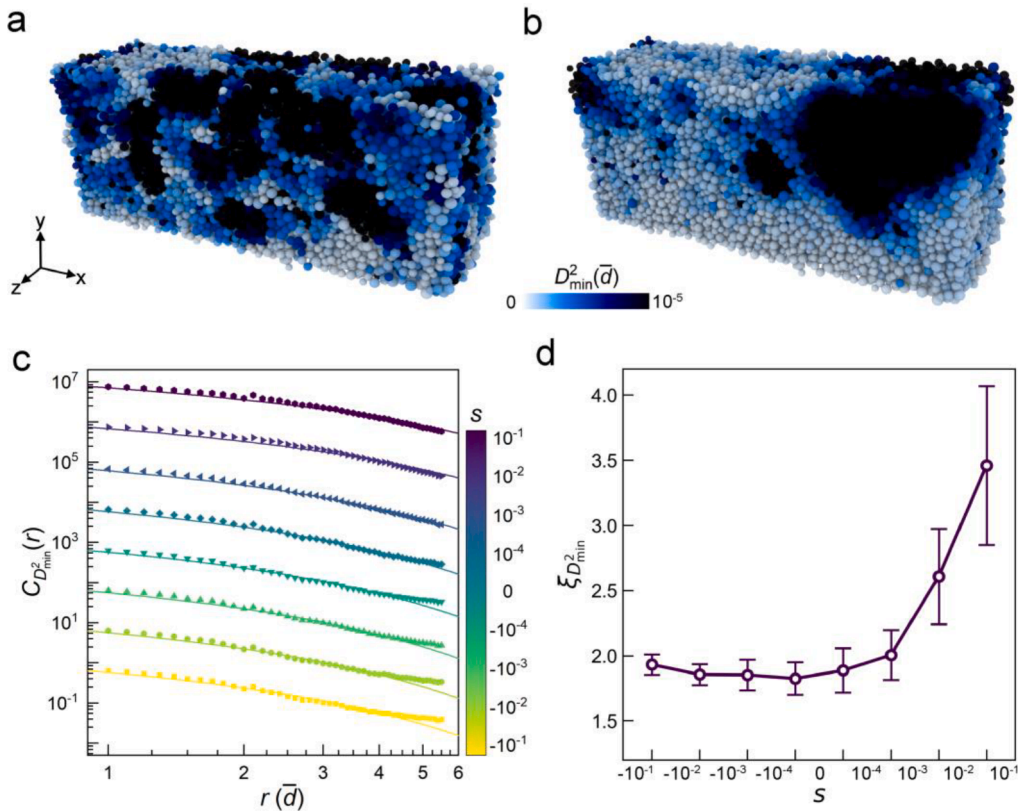
Fig. 2. Spatial analysis of microscopic dynamics. **(a)** and **(b)** respectively show the snapshot of the squared nonaffine displacement D_{min}^2 during the stick and slip stages of a typical slip avalanche event. **(c)** The spatial correlation function of D_{min}^2. The data points are averaged over the stick or slip stages falling into each bin and the color codes the magnitude of stress fluctuation during a target stage. Solid lines are fits using the Ornstein-Zernike function as $C_{D_{min}^2}(r) \sim r^{-0.5} \exp(-r/\xi_{D_{min}^2})$. The data points and fitting lines of different bins are shifted vertically for better visualization. **(d)** Spatial correlation length $\xi_{D_{min}^2}$ versus stress fluctuation s.

3. Results

3.1. Spatial correlation of microscopic dynamics

As illustrated in the Introduction part that particles tend to undergo collective dynamics behavior under external stimuli, we start by investigating the spatial correlation of microscopic dynamics. Fig. 2a and 2b respectively show the spatial distributions of D_{min}^2 during the stick stage and slip stage of a typical stick-slip cycle. Particles with higher D_{min}^2 are colored with black. Due to the discrete nature of granular materials, the localized microscopic dynamics manifests a collective and cooperative behavior, which is believed to be the fundamental building block of plasticity in granular materials (Budrikis et al., 2017; Ma et al., 2021). Intuitively, microscopic dynamics is scattered throughout the granular system during the stick stage. During the slip stage, the microscopic dynamics is more spatially concentrated and tends to generate large clusters inside the granular system. To gain a deeper understanding of the difference among stages with different stress fluctuations, we further quantify the spatial correlation of D_{min}^2 using the normalized spatial correlation function (Cubuk et al., 2017; Karimi et al., 2019),

$$C_{D_{min}^2}(r) = \frac{\sum_{i=1}^{N}\sum_{j=1}^{N}\Delta D_{min,i}^2 \Delta D_{min,j}^2 \delta(r - r_{ij})}{\sum_{i=1}^{N}\sum_{j=1}^{N}\delta(r - r_{ij})} \qquad (5)$$

where the bracket $\langle \bullet \rangle$ denotes averaging over all particles. where $C_{D_{min}^2}(r)$ denotes the spatial correlation coefficient of D_{min}^2 over a distance r, N is the number of particles in the granular assembly, r_{ij} denotes the distance between particles i and j, the Kronecker delta $\delta(r - r_{ij}) = 1$ if and only if $r - r_{ij} = 0$, and
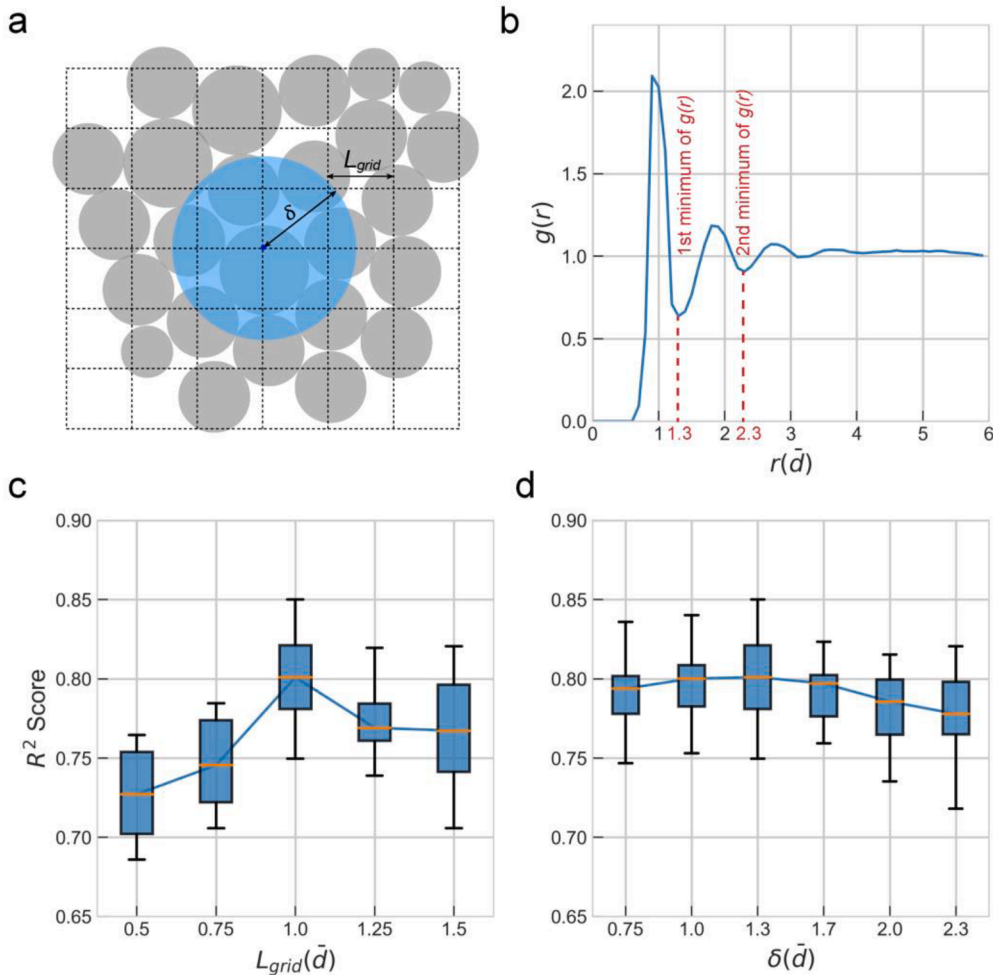
Fig. 3. From disorder to order. **(a)** Schematic of the proposed coarse-graining method. **(b)** Pair correlation function $g(r)$ of the granular system. The influence of L_{grid} and δ on the performance of CNN model is shown in **(c)** and **(d)**, respectively.

$$\Delta D^2_{\min,i} = D^2_{\min,i} - \frac{1}{N}\sum_{k=1}^{N} D^2_{\min,k} \qquad (6)$$

is the fluctuation of the squared nonaffine displacement of particle i with respect to its mean value over the whole assembly. We group the stick and slip events according to the magnitude and sign of stress fluctuation. Logarithmic binning is used. As shown in Fig. 2c, the spatial correlations represented by scatters decay rapidly within a short distance of several $\bar{d}$, where $\bar{d}$ denotes the mean particle diameter. The solid lines in Fig. 2c indicate that the decay of $C_{D^2_{\min}}(r)$ can be well fitted by the Ornstein-Zernike function as $C_{D^2_{\min}}(r) \sim r^{-0.5}\exp(-r/\xi_{D^2_{\min}})$ (Kawasaki et al., 2007), and we can obtain the spatial correlation length $\xi_{D^2_{\min}}$. We further show in Fig. 2d the evolution of $\xi_{D^2_{\min}}$ versus stress fluctuation. The correlation length $\xi_{D^2_{\min}}$ remains nearly unchanged during stick stages and increases rapidly for large slip events, which indicates that the varying magnitudes of macroscopic stress fluctuations may be controlled by the different spatial patterns of particle dynamics, providing the basis for linking particle-scale dynamics and macroscopic response through DL.

3.2. 3D cnn links particle dynamics to macroscopic response

Here, we start by using DL to estimate the macroscopic response of granular assembly. Specifically, we rely exclusively on the spatial patterns of microscopic dynamics during given stages, with a goal of inferring corresponding macroscopic stress fluctuations. It is worth noting that the stress fluctuation is just an example of target and our method is also applicable for building similar micro-macroscopic relationships.

How to gather the dynamic information of every single particle and extract key information is a difficult task for such a complex system. In addition, due to the fact that microscopic dynamics is spatially correlated (Xia et al., 2015), it is also important to take the spatial information of particle dynamics into account. Many existing works have revealed that CNN is capable of automatically detecting important spatial characteristics without any human supervision, making CNN the go-to model in many fields such as computer vision (He et al., 2016) and natural language processing (Chowdhary, 2020). Therefore, we propose a 3D CNN-based framework for linking particle dynamics and macroscopic response in this paper. Since CNN only handles structured data, the disordered granular assembly is firstly converted to a voxel matrix via a coarse-graining method. As shown in Fig. 3a, the coarse-graining method first sets a regular distributed grids with a spacing of L_{grid}, and then assigns every grid the average value of $D^2_{\min}$ of particles within the region of radius δ around it. Fig. 3b shows the pair correlation function $g(r)$, where the first and second minimum correspond to the first- and second-neighbor shell of a given particle. As shown in Fig. 3c and 3d, the combination of $L_{grid} = 1.0d_{50}$ and $\delta = 1.3d_{50}$ yields the best performance and is therefore used in this paper.

The resulted voxel matrix, similar to a picture made up of pixels, contains many individual "blocks" of the same size, which is fed into the downstream CNN framework to train and predict the macroscopic stress fluctuations of granular assembly (see Fig. 4). Fig. 4 also shows the architecture of the 3D CNN containing of two components that operate sequentially, i.e. convolution layers for feature
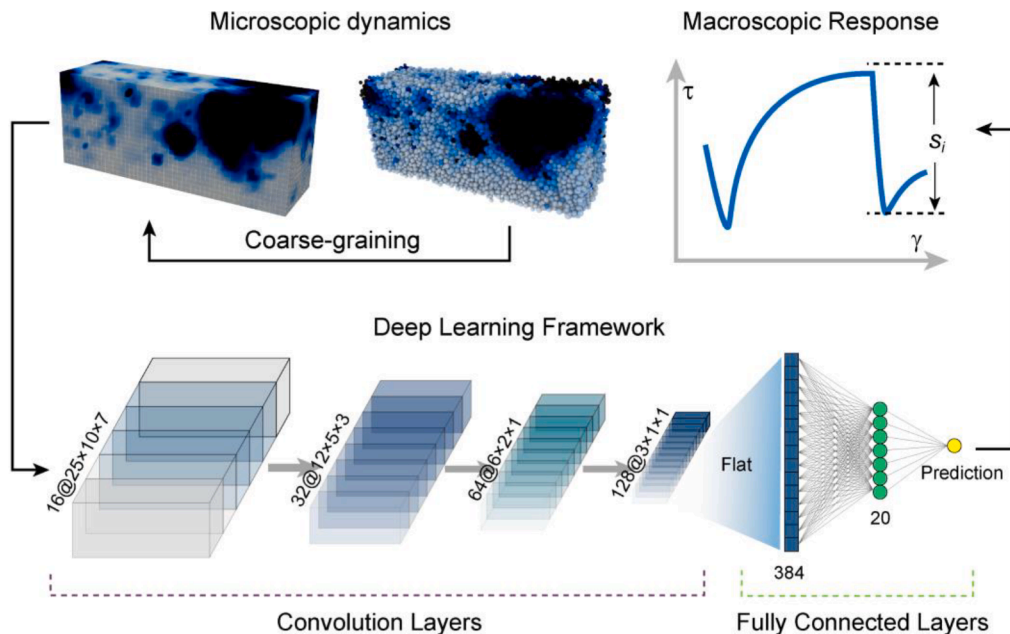
Fig. 4. Schematic of the 3D Convolution Neural Network (CNN) model consisting of convolution layers and fully connected layers. The set of boxes represents the feature map. The size of the feature map is denoted upon each feature map.

extraction and fully connected layers for parameter regression. Specifically, the CNN model consists of four convolutional layers with a kernel size of $3 \times 3 \times 3$, where $f = \{16, 32, 64, 128\}$ is the number of channels of the $i - th$ layer. The number of channels denotes the number of convolution kernels of the corresponding convolution layer. The convolutional layers are used for extracting spatial patterns of microscopic dynamics. Following every convolutional layer, a MaxPooling layer with a kernel size of $2 \times 2 \times 2$ is applied to reduce the data. After the MaxPooling layer, the feature maps are fed into the rectified linear unit (ReLU) activation function to achieve nonlinearity. Finally, the fully connected layers are applied to reduce feature maps and get the final prediction. It is worth noting that the 3D CNN in this paper is implemented using the Python Pytorch Package (Paszke et al., 2019).

During the shearing process, a total of 4232 slip avalanches (stick-slip cycles) are recorded and used to construct the DL dataset. That is, a total of 8464 samples are included. As shown in Fig. 5a, the dataset is divided into the training set, validation set and test set, with a proportion of 60%, 20% and 20%, respectively. These three sets are used for training CNN, tuning the hyperparameters of CNN and evaluating CNN, respectively. The loss function used for training the CNN model is the mean square error (MSE). We further show in Fig. 5b the evolution of the training and test loss during the training process of CNN, and the final prediction performance on the
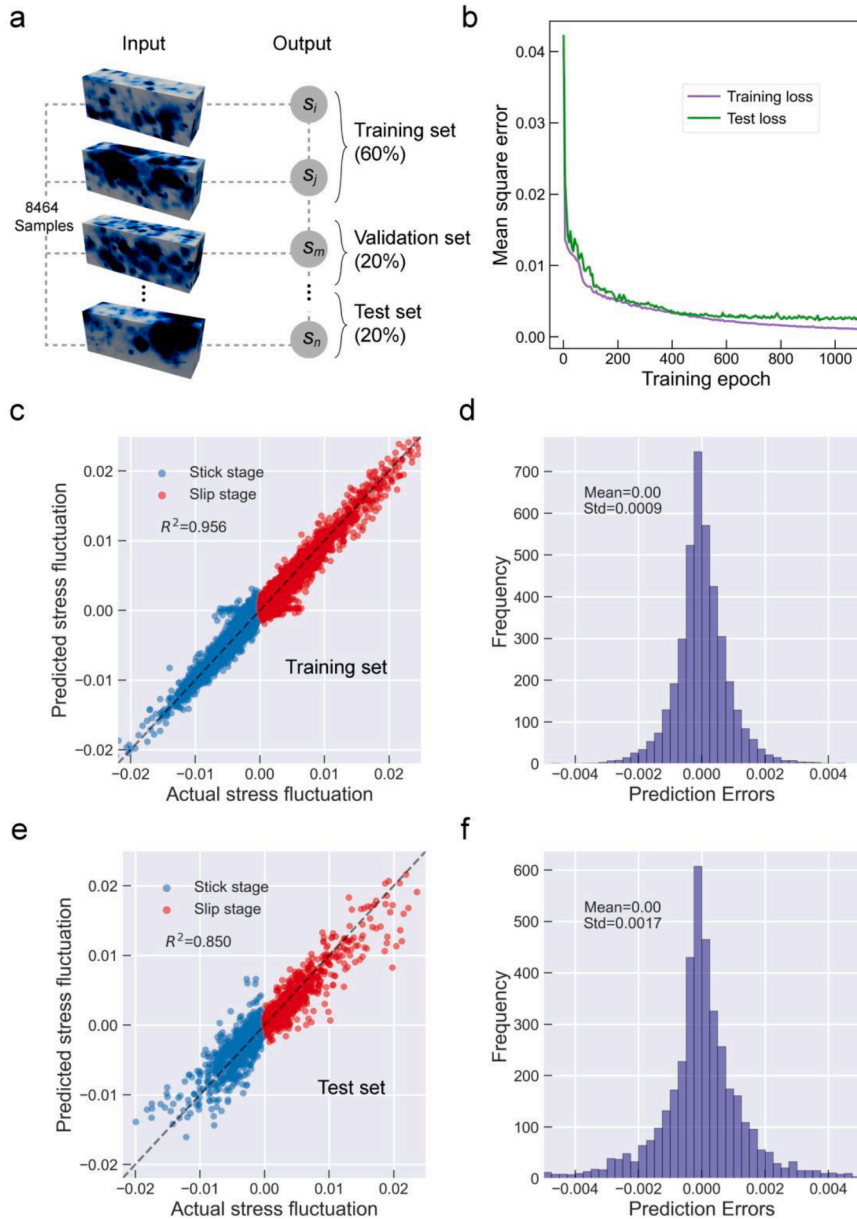
Fig. 5. Predicting stress fluctuations using microscopic dynamics and deep learning. **(a)** The division of the DL dataset. **(b)** Training and test errors during the training process of the CNN model. **(c)** and **(e)** show the prediction performance of CNN for the training set and the test set, respectively. **(d)** and **(f)** show the frequency of prediction errors for the training set and the test set, respectively.

training set and the test set are shown in Fig. 5c and 5e, respectively. The proposed CNN model can not only classify the stick and slip stages from microscopic dynamics, but also predict the magnitudes of stress fluctuations with high accuracy. As a quantitative description, the coefficient of determination R^2 between actual and predicted stress fluctuations is 0.956 for the training set and 0.85 for the test set. We further show in Fig. 5d and 5f the frequency of prediction errors with a mean error close to zero and a small standard deviation. These results illustrate that the proposed 3D CNN indeed establishes a quantitative linkage between microscopic dynamics (or particle-scale dynamics) and macroscopic stress fluctuations. In our previous work, a machine learning-based approach is proposed to link the statistical features of microscopic behaviors to macroscopic responses (Ma et al., 2022). However, machine learning-based approaches strongly rely on the hand-crafted statistical features, the definition of which needs human intervention. When encountering other questions with little prior knowledge, the feature-extracting process usually handers the model performance, which will lower the applicability of the machine learning approach to the study of other amorphous solids. More importantly, the hand-crafted
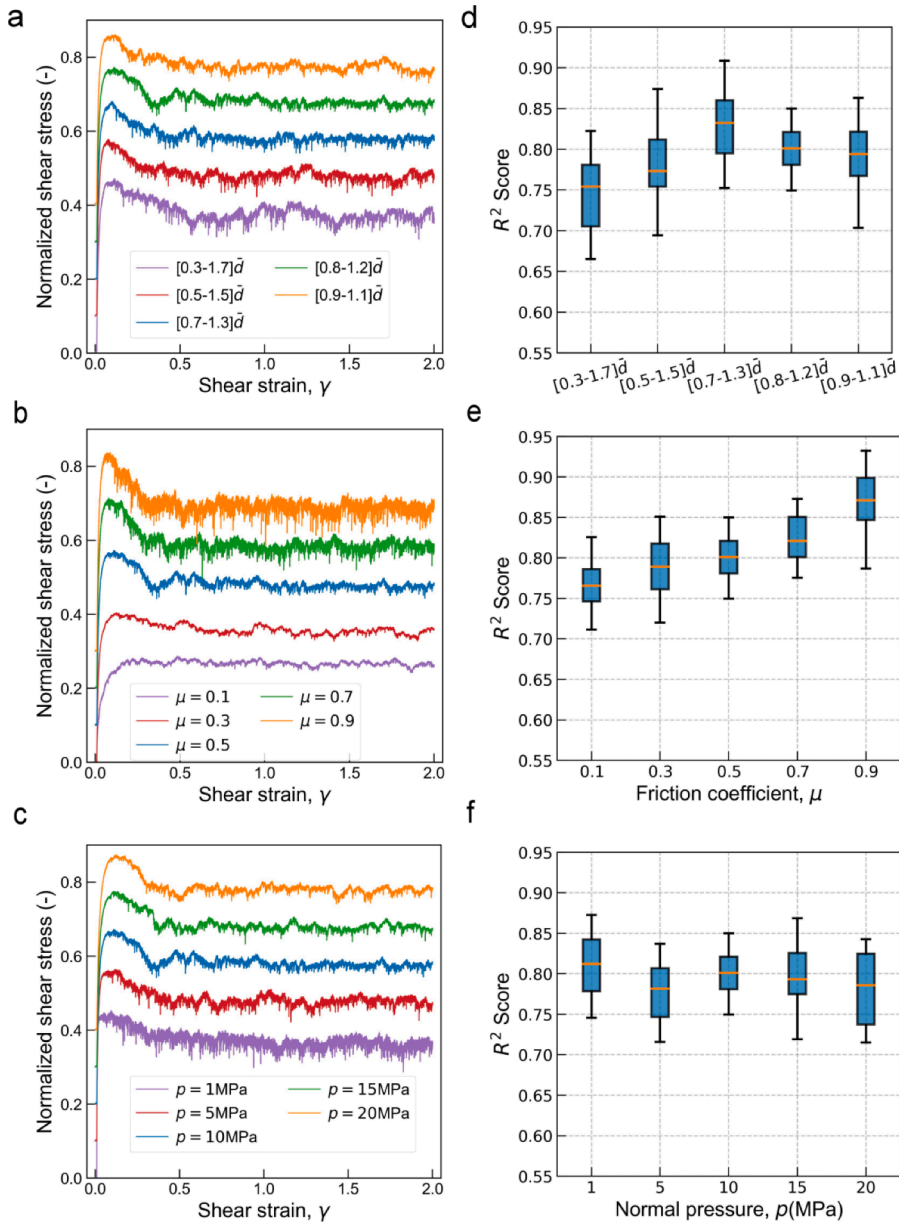
Fig. 6. Prediction performances of the CNN model over different granular systems. Prediction performances of the CNN model over different granular systems. Stress-strain curves of granular systems with **(a)** different size distributions, **(b)** different inter-particle friction coefficients, and **(c)** different normal pressures. The curves have been shifted vertically to facilitate visual inspection. The prediction performances of the CNN model are shown for granular systems with **(d)** different particle size distributions, **(e)** different inter-particle friction coefficients, and **(f)** different normal pressures.

statistical features hamper the acquisition of novel knowledge and our further understanding into the underlying relationship between microscopic dynamics and macroscopic responses. In this context, the proposed CNN model can automatically detect important spatial features at the particle scale and predict macroscopic responses without the requirements of a priori knowledge, self-defined statistical features, and human supervision, which can greatly facilitate our ability to obtain novel knowledge from the data-driven process. Moreover, the flexibility of CNN model enables the deep-learning framework can be more easily extended to future studies of other amorphous solids.

3.3. Generalization of the cnn model

As we mentioned in the Introduction part, the slip avalanche phenomenon and its related statistical features can be tuned by many parameters, such as the particle size polydispersity (Ma et al., 2020), the inter-particle friction coefficient (Dorostkar and Carmeliet, 2019) and the normal pressure (Gao et al., 2020). To further demonstrate the applicability of the proposed CNN framework for building the quantitative relationship between microscopic dynamics and macroscopic responses, we perform more numerical tests of granular systems with different simulation parameters (see Fig. 6a to 6c). Specifically, five particle size distributions are considered, i. e., particle diameters uniformly distributed on the interval $0.3 - 1.7\bar{d}$, $0.5 - 1.5\bar{d}$, $0.7 - 1.3\bar{d}$, $0.8 - 1.2\bar{d}$ and $0.9 - 1.1\bar{d}$. Five levels of inter-particle friction coefficients μ are considered, i.e., 0.1, 0.3, 0.5, 0.7 and 0.9, and five levels of normal pressures p are also considered, i.e., 1 MPa, 5 MPa, 10 MPa, 15 MPa and 20 MPa. We repeat the above operations and obtain the prediction accuracy of 3D CNN on these granular systems. As illustrated in Fig. 6d to 6f, the proposed CNN model yields satisfactory performances over all these
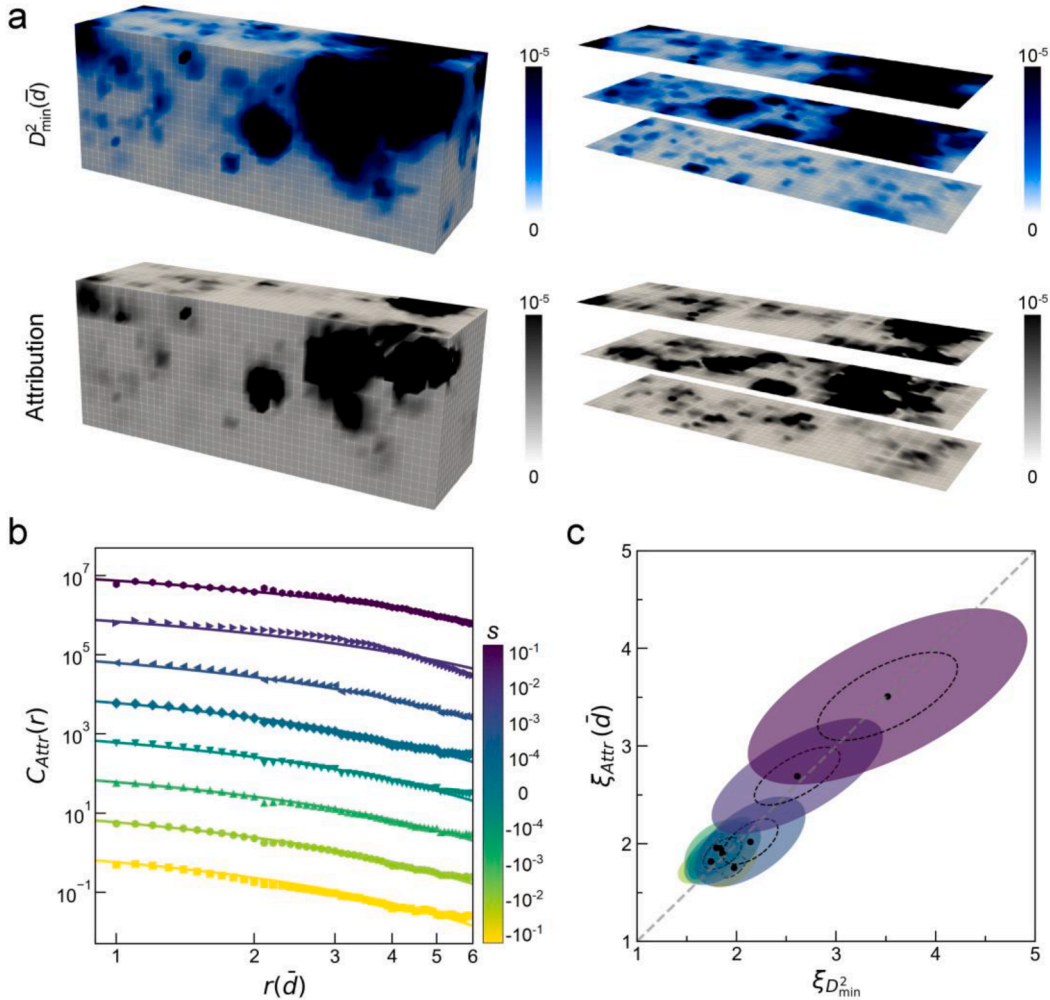
Fig. 7. Interpretation of CNN. **(a)** Snapshots and typical slices of $D^2_{\min}$ and attribution fields for a typical slip event. **(b)** The spatial correlation of attribution, ξ_{Attr}. The data points and fitting lines of different bins are shifted vertically for better visualization. **(c)** Parameter space for $\xi_{D^2_{\min}}$ and ξ_{Attr}. The dotted (solid) ellipses around each best fit ($\xi_{D^2_{\min}}$, ξ_{Attr}) are the 1σ (2σ) confidence regions as determined by 200 randomly chosen events. The dashed line is a guide to the eye with a slope of 1.0.

systems, indicating that the proposed CNN framework to connect microscopic dynamics and macroscopic responses is indeed applicable to a broad range of granular systems.

4. Discussions

4.1. Interpretation of 3D cnn

As previously noted, while the previous ML method (Ma et al., 2022) and the CNN model in this work can build the quantitative relationships between microscopic dynamics and macroscopic responses in some ways, this is just the first step to building and understanding the multiscale relationships within granular materials, and many fundamental questions remain elusive, including but not
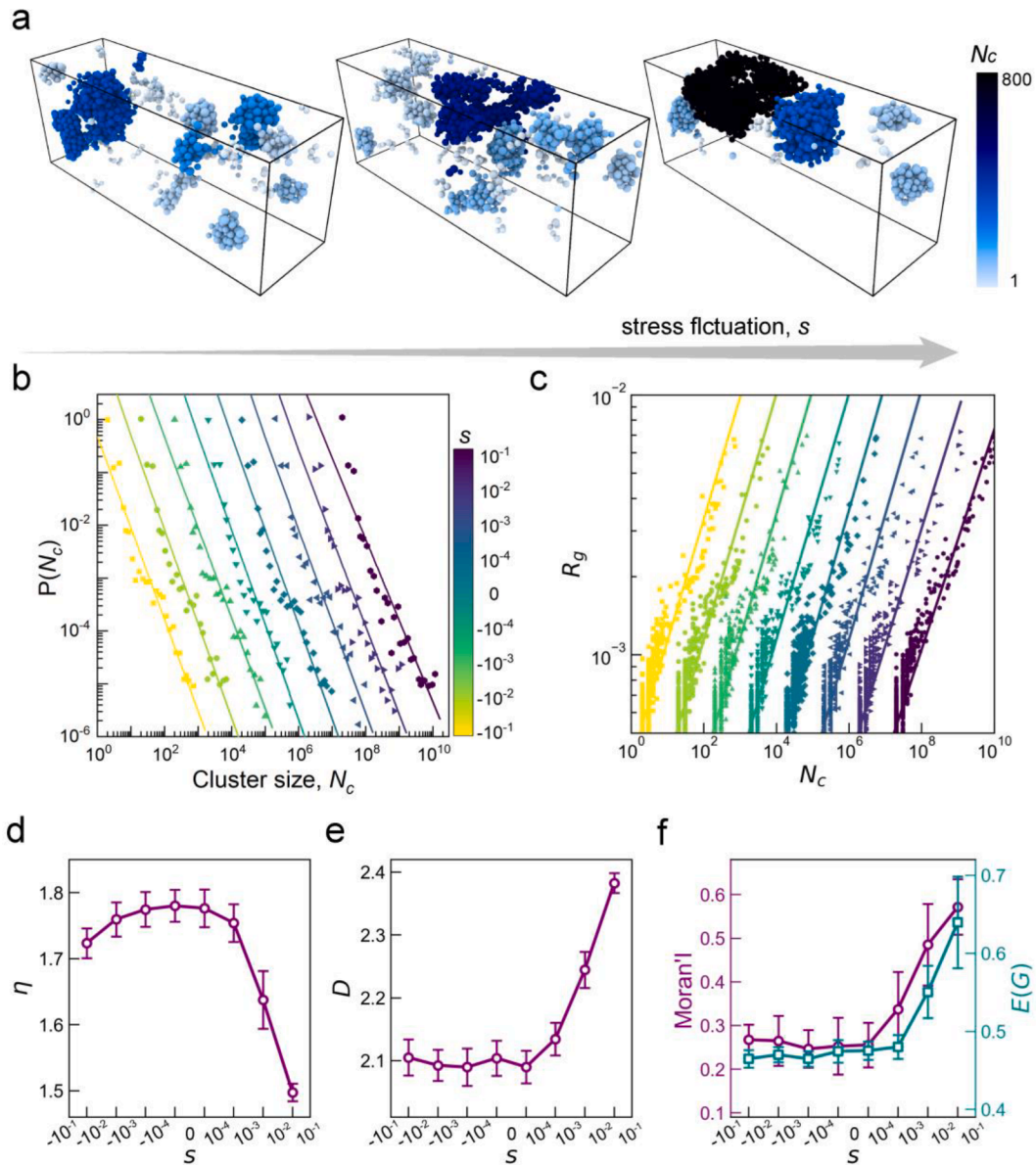
Fig. 8. Clustering analysis of microscopic dynamics. **(a)** Snapshots of active particle clusters (top 10% of $D_{\min}^2$) with the increase of stress fluctuation. Clusters smaller than three are not shown in this figure for better visualization. **(b)** PDFs of cluster size N_c. Solid lines are fits using the power-law function $P(N_c) \sim N_c^{-\eta}$. The data points and fitting lines of different bins are shifted horizontally for better visualization. **(c)** Radius of gyration of the active clusters versus N_c. Solid lines are fits using the power-law function $R_g \sim N_c^{1/D}$. The data points and fitting lines of different bins are shifted horizontally for better visualization. **(d)** Evolution of power-law exponent η with stress fluctuation s. **(e)** Evolution of the fractal dimension D as a function of stress fluctuation s. **(f)** Global Moran' I and global efficiency $E(G)$ versus stress fluctuation s.

limited to what type of spatial information is important for the predictions, whether there are some mesoscopic structures responsible for varying macroscopic responses, and what causes the different spatial patterns of mesoscopic structures, etc. Answering these questions is vital for revealing the origin of complex behaviors and understanding multiscale relationships of granular materials. To this end, we need to first reveal what pattern memorized by 3D CNN to make the predictions. In other words, whether 3D CNN relies on different spatial patterns of microscopic dynamics to make predictions needs to be further interpreted. But due to its multilayer nonlinear structure, CNN has a longstanding drawback of acting like a black box in the sense that it is not clear how and why it arrives at a particular prediction (Montavon et al., 2017). Here we employ the Integrated Gradients Method (IGM) to interpret the proposed CNN model. IGM computes the gradient of the prediction output regarding features of the input, and the gradient is treated as the attribution of the corresponding feature. Detailed information about IGM can be found in the original paper (Sundararajan et al., 2017).

In our case, every grid of a voxel matrix is assigned a value named "attribution" representing the importance with respect to the predicted stress fluctuation. Fig. 7a shows the snapshots of D_{min}^2 and the attribution fields of a typical slip stage, where the volumes and the horizontal slices of these two variables show similar spatial distributions. We then quantify the spatial correlation of the attribution using the normalized spatial correlation function as shown in Fig. 7b. Following the above calculation of $\xi_{D_{min}^2}$, we also calculate the correlation length of attribution, ξ_{Attr}. As illustrated in Fig. 7c, the correlation length of microscopic dynamics, $\xi_{D_{min}^2}$, and the correlation length of attribution, ξ_{Attr}, fall on a dashed line $\xi_{Attr} / \xi_{D_{min}^2} = 1.0$ for bins with different stress fluctuations. Thus, $\xi_{D_{min}^2}$ and ξ_{Attr} are strongly correlated. Our 3D CNN interpretation analysis provides compelling evidence that the size of attribution is identical to the size of microscopic dynamics, which indicates that the proposed 3D CNN approach precisely utilizes the spatial patterns of microscopic dynamics to predict the macroscopic stress fluctuations.

4.2. Spatial clustering of microscopic dynamics

From the above interpretation of CNN, the particles carrying large D_{min}^2 aggregate together to form clusters (Kou et al., 2018) and are generally assigned large attributions (see Fig. 7a). Thus, clusters formed by particles with strong dynamics behavior (active particles) play an important role in inferring macroscopic responses. Similar to previous studies regarding the percolation analysis of active particles (Hamedmoghadam et al., 2021; Kou et al., 2018; Xia et al., 2015), we extract the top 10% highest D_{min}^2 particles as active particles for cluster analysis. Fig. 8a shows three typical snapshots of active particle clusters with the increase of stress fluctuation. The clusters are colored according to cluster size N_c, i.e., the number of particles they contain (see the colorbar of Fig. 8a). Intuitively, the granular assembly tends to generate larger clusters with the increase of stress fluctuation. We further show the PDFs of cluster size $P(N_c)$ for stick and slip events of different magnitudes in Fig. 8b. The PDFs are linear in the log-log plot, suggesting a power-law decay $P(N_c) \sim N_c^{-\eta}$. A larger η indicates more small clusters. The magnitude-dependence of η is clearly illustrated in Fig. 8d, where η remains nearly unchanged for the stick stages but decreases rapidly for large stress drops. This indicates that a more cooperative and concentrated distribution of microscopic dynamics in space constitutes the microscopic origin of global slip avalanche.

To further quantify the geometry of active particle clusters, we define the radius of gyration R_g of a cluster as

$$R_g^2 = \frac{\sum_{i=1}^{N_c} V_i (\mathbf{r}_i - \overline{\mathbf{R}})^2}{\sum_{i=1}^{N_c} V_i} \tag{7}$$

where the summation is carried over N_c particles belonging to the cluster, $\mathbf{r}_i$ is the position of particle i, and $\overline{\mathbf{R}}$ is the center of the cluster. The N_c dependence of R_g for clusters is shown in Fig. 8c, showing that the radius of gyration R_g has a power-law growth with the cluster size s, i.e., $R_g \sim N_c^{1/D}$. For $D <$ dimensionality (3 in this case), the clusters are not space-filling and have a fractal structure (Ghosh et al., 2017). The evolution of fractal dimension D versus stress fluctuation is illustrated in Fig. 8e. The fractal dimension increases with the increasing magnitude of stress fluctuations for drop stages, indicating the decreasingly fractal-like packings of active clusters.

However, the cluster size distribution and gyration radius contain no information about the spatial distribution of active clusters. Therefore, we introduce two metrics to describe the spatial pattern of active clusters, i.e. the global Moran' I and the global efficiency $E(G)$. Specifically, the global Moran' I is defined as

$$I = \frac{N}{W} \frac{\sum_{i=1}^{N} \sum_{j=1}^{N} w_{ij} (a_i - \overline{a})(a_j - \overline{a})}{\sum_{i=1}^{N} (a_i - \overline{a})^2} \tag{8}$$

where N is the number of particles, w_{ij} is the spatial weight between particle i and j, W is the sum of all w_{ij}, a_i denotes whether particle i belongs to active clusters, and a_i equal 1 if particle i belongs to active clusters, else 0. In this case, the global Moran' I, ranging from 0 to 1, measures the overall spatial autocorrelation of active clusters, and larger values indicate a more spatially correlated pattern of active clusters. On the other hand, the calculation of the global efficiency is derived from the graph theory. Graph refers to a pictorial representation of a set of objects where links connect some pairs of objects (Papadopoulos et al., 2018). The objects are termed nodes, and the links that connect the nodes are called edges. The main assumption is that the more distant two nodes are in the graph, the less efficient their communication will be. The global efficiency $E(G)$ can be calculated as

$$E(G) = \frac{1}{N(N-1)} \sum_{i \neq j \in G} \frac{1}{d_{ij}}$$

(9)

where N denotes the number of nodes, d_{ij} is the length of the shortest path between node i and node j. In this case, the assembly of active clusters are constructed as a graph, where each cluster is treated as a node at its center, and each cluster is assigned an edge with each of its three nearest clusters. We note that the number of neighbors does not influence the result of this study. The edge connecting two clusters are characterized by the distance between the centers of clusters, which is considered when calculating the shortest path between two clusters. A larger global efficiency indicates that the distribution of active clusters is more concentrated over space.

Fig. 8f show the evolutions of Moran' I and $E(G)$ with stress fluctuation s. Moran' I and $E(G)$ remain nearly unchanged during stick stages and gradually increase with the stress fluctuation during drop stages, implying significantly different spatial patterns where active clusters distribute dispersedly over space during stick stages and turn to get together during drop stages. Previous studies employed the Moran Index to quantify the heterogenous degree of the strain filed, and it is found that the Moran Index continuously increases till the formation of the final shear band, suggesting the cooperative evolution between the shear strain field and the dynamic heterogeneity (Liu et al., 2018; Zhu et al., 2016b). This is also reminiscent of the experimental investigation of the yield transition in colloidal glasses (Ghosh et al., 2017), in which the spatial clusters of microscopic dynamics are found to grow during the external shearing process and finally percolate over the system when approaching the critical yield point. These findings may suggest the universal nature of the critical behavior and the mechanical failure of amorphous solids from the perspective of microscopic dynamics. Thus, it is of vital importance for future works to investigate the spatial organization of microscopic dynamics and its critical behaviors till the occurrence of slip avalanches. Taken together, the spatial and clustering analyses suggest different underlying mechanisms of microscopic dynamics governing macroscopic stress fluctuations, and the spatial pattern of microscopic dynamics is the "fingerprint" of the macroscopic response of granular materials.
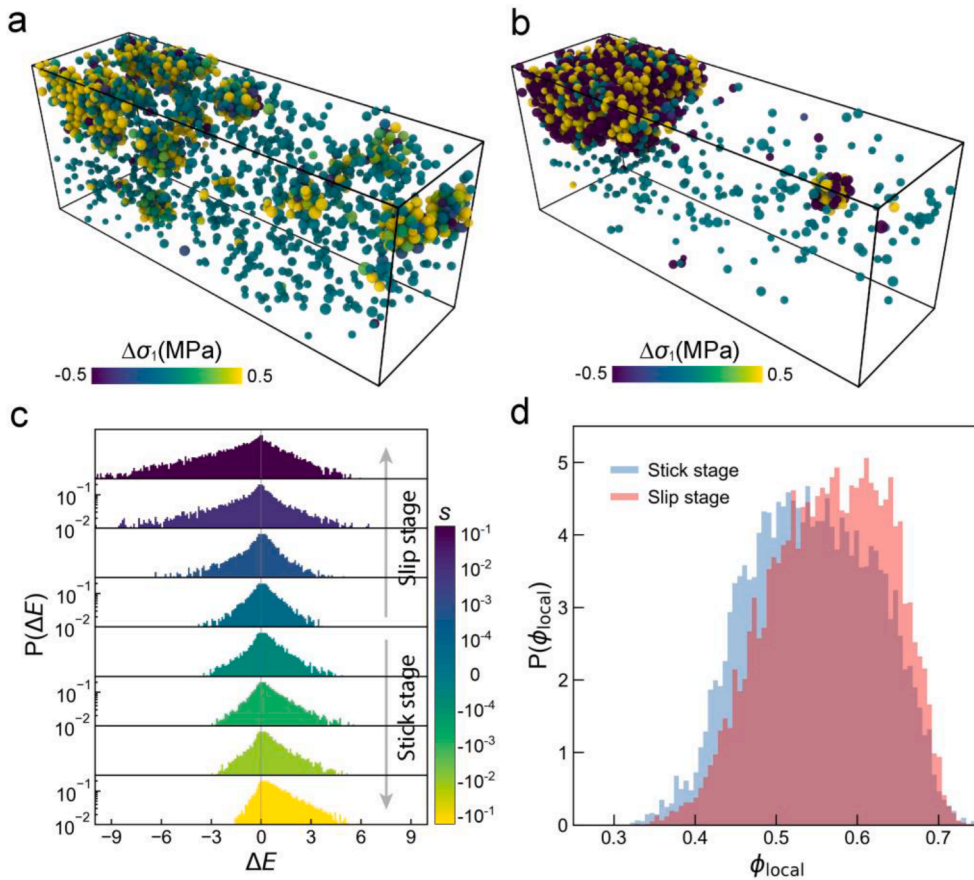
Fig. 9. Different modes of microscopic dynamics. **(a)** and **(b)** respectively show snapshots of $\Delta\sigma_1$ during the stick stage and the slip stage of a typical avalanche event. **(c)** The probability distributions of ΔE during stages with different magnitudes of stress fluctuations. Note that ΔE is rescaled by its mean value. **(b)** Comparison of the PDFs of local packing fraction ϕ_{local} during the stick and slip stages. Data are averaged over all frames of every stage.

4.3. Different causes for microscopic dynamics

The above analysis reveals the significantly different spatial modes of microscopic dynamics during stick and slip stages, suggesting differently underlying causes for the microscopic dynamics. In this part, we take a deeper investigation into the different causes of microscopic dynamics. There is a general consensus that particles form a highly heterogeneous contact network, providing support for external loading (Krishnaraj and Nott, 2020; Zhu et al., 2016a). In addition, many existing works have revealed that the stick-slip behavior of granular materials can be seen as a jamming-unjamming process or phase transition (Ramola and Chakraborty, 2017), accompanied by the formation, buckling and breakage of force chains (Tordesillas, 2007). Thus, the dynamics of contact networks play an important role in the macroscopic response of granular assembly and may be related to different modes of microscopic dynamics.

Here we also take the top 10% highest $D_{\min}^2$ particles as active particles for the following analysis. With the aid of computer simulation, we are able to calculate the particle stress tensor by averaging discrete contact forces around one particle into an equivalent continuum stress tensor (Love, 1927; Nicot et al., 2013; Zhu et al., 2016a). Specifically, the stress tensor of particle p is defined as:

$$\sigma_{ij}^p = \frac{1}{V_p} \sum_{c=1}^{N_c^p} f_i^c v_j^c \tag{10}$$

where N_c^p denotes the number of contacts to the particle p, for a contact c, f_i^c is the ith component of the contact force to the particle, v_j^c is the jth component of the contact vector connecting the center of particle p to the contact point, and V_P is the volume of the particle p. The direction of the major eigenvector of σ_{ij}^p represents that of the force transmission across particle p, and the corresponding major principal stress σ_1^p (compressive positive) is often used in the characterization of force chains and the identification of buckling events (Liu et al., 2020; Zhu et al., 2016a). We then quantify the local stress dynamics using the fluctuation of major principal stress $\Delta\sigma_1$ over each stage. Snapshots of $\Delta\sigma_1$ during the stick and slip stages of a typical slip avalanche are shown in Fig. 9a and 9b, respectively. Active particles of the slip stage suffer higher stress fluctuation, while those of the stick stage are mainly dispersed throughout the packing with lower stress fluctuation.

The dynamics of contact network can be further investigated from the perspective of particle-scale potential energy (Dorostkar and Carmeliet, 2018; Ma et al., 2020; Zheng et al., 2018). The elastic potential energy is stored in particles through the particle deformation at contacts. Thus, the normal and tangential stored energies at contact c are calculated by

$$E_n^c = \int_0^{\Delta_n} f_n(\delta_n)d\delta_n = \frac{4(3/4f_n)^{5/3}}{15(E^*)^{2/3}(R^*)^{1/3}} \tag{11}$$

$$E_t^c = \int_0^{\Delta_t} f_t(f_n(\delta_n),\delta_t)d\delta_t = \frac{(f_t)^2(1+v)(2-v)}{8E^*a} \tag{12}$$

where f_n and f_t are the magnitudes of normal and tangential forces, δ_n and δ_t are the overlapping and tangential deformation between contacting particles. $E^* = E/(2(1-v^2))$, where E and v are Young's modulus and Poisson's ratio. $R^* = r_1 r_2/(r_1 + r_2)$, where r_1 and r_2 are the radii of the two contacting particles. a is the contact radius calculated by the Hertzian contact theory. The total energy stored in the system is then given by $E_{pot} = \sum_{k=1}^{N_c}(E_{k.n}^c + E_{k.t}^c)$, where N_c is the total number of contacts. The particle scale elastic potential energy is calculated by

$$E_i = \sum_j^{N_i} 0.5\left(E_{j,n}^c + E_{j,t}^c\right) \tag{13}$$

where the summation takes over the N_i contacts of particle i. The fluctuation of particle-scale potential energy during a given stage provides a quantitative diagnosis for the dynamics of contact network, and we show in Fig. 9c the PDFs of particle-scale potential energy fluctuation ΔE. For all bins, the probability distributions of energy fluctuations ΔE all show a Boltzmann-type, double-exponential distribution for both $\Delta E > 0$ and $\Delta E < 0$. Furthermore, the active particles of slip stages are obviously suffering stronger contact network dynamics.

We further show the PDFs of local packing fraction ϕ_{local} during the stick and slip stages in Fig. 9d. The local packing fraction is calculated as $\phi_{local} = V_p/V_{voro}$, where V_p and V_{voro} are the particle volume and its Voronoi cell volume, respectively. As shown in this figure, active particles during stick stages occupy more free volume than slip stages. Token together, our analysis reveals different causes for microscopic dynamics It is reasonable to conclude that microscopic dynamics of slip stages has a high propensity to directly originate from contact network dynamics. When it comes to the stick stages, microscopic dynamics is mainly manifested as the free volume-induced structure rearrangement, i.e. irreversible reconfiguration of particle site environment and redistribution of free volume within the neighbor shells (Li et al., 2013). That is, during the stick stages, the active clusters of spatially dispersed distribution are because the sites with large free volumes are scattered throughout the system. In contrast, during the slip stages, the active clusters of spatially concentrated distribution are induced by the sudden adjustment of the contact network, which acts as a point-source excitation and causes the cooperative dynamic behaviors of the neighborhood particles.

5. Concluding remarks

In summary, this work forms the first CNN-based framework to quantitively link particle-scale dynamics to macroscopic responses of the granular system. The data-driven framework can efficiently extract the dynamic information at the microscopic scale and their spatial correlation. The generalization power of this 3D CNN model is verified over granular assemblies with different size polydispersity, different shear rates, and different friction coefficients, indicating the proposed data-driven framework is capable of modeling the multiscale relations for a broad range of granular systems. To understand how a prediction is made by the deep learning framework, a model interpretation module is introduced to reveal the different contributions of different sites within the granular assembly to the prediction of macroscopic responses. With such an interpretation module, this work provides the first quantitative and direct evidence that the mesoscopic structures, i.e., active clusters with high microscopic dynamics, are responsible for the macroscopic responses, and the spatial pattern of microscopic dynamics acts as the "fingerprint" of macroscopic responses and controls the magnitude of stress fluctuations. Two different mechanisms are further to be responsible for the different spatial patterns of microscopic dynamics during the stick and slip regimes, i.e., free volume-induced structural rearrangements for the stick regime and contact network dynamics for the slip one. These findings are of vital importance for understanding the complex plastic behaviors (Jiang et al., 2020; Nicolas et al., 2018; Nicot et al., 2012) and achieving better predictions of the exact occurrence time of slip avalanches (Ferdowsi et al., 2013; Johnson et al., 2021; Shreedharan et al., 2020).

We believe the data-driven framework proposed in this work may shed some light on future constitutive modeling of granular materials. Specifically, previous studies usually rely on fully connected neural networks (FCNNs) or recurrent neural networks (RNN) to capture the temporal correlation of self-defined variables and to predict the history-dependent mechanical behaviors of granular materials (Bahmani and Sun, 2022; Guan et al., 2022; Karapiperis et al., 2021; Qu et al., 2021; Wang and Sun, 2018). While several internal variables are usually used to reflect the micromechanical information in these studies, they are defined or averaged over the whole assembly. They may miss important details at the particle scale. This data-driven framework proposed in the paper can automatically detect important spatial features of dynamic behaviors at the individual particle scale and predict the macroscopic responses without any human supervision. It can be combined with the abovementioned approaches to provide complete internal information into the constitutive modeling of granular materials. For example, one may combine the CNN model for extracting the particle-scale dynamic behaviors and their spatial correlation with the RNN model for capturing their temporal evolution. Such an architecture may enable us to model the constitutive behaviors of granular materials with higher accuracy and reproduce the intermittent dynamic behavior, which is often ignored in previous studies.

Furthermore, it is a longstanding topic on building multiscale relations linking particle-scale property with the macroscopic response of amorphous solids. However, due to the intrinsically disordered and heterogeneous structure and complex multibody interaction, extracting key microscopic information of such complex systems is difficult (Mungan et al., 2019; X. Wang et al., 2021). Along with the model interpretation technique, we believe the data-driven framework together with the model interpretation module proposed in this paper should be applicable and easily extended to a wide range of amorphous materials such as metal glasses for understanding and building multiscale relations. Thus, we can deepen the understanding of key scientific issues such as the micro-macroscopic relationship, and gain novel insight into the mechanical properties of such materials.

Data availability

The datasets used in the current study can be available from the corresponding author on reasonable request.

CRediT authorship contribution statement

Jiangzhou Mei: Conceptualization, Methodology, Software, Investigation, Writing – original draft, Formal analysis. **Gang Ma:** Conceptualization, Methodology, Validation, Data curation, Writing – review & editing, Visualization. **Longwen Tang:** Validation, Formal analysis, Writing – review & editing, Supervision. **Ke Gao:** Validation, Writing – review & editing. **Wanda Cao:** Validation, Visualization. **Wei Zhou:** Visualization, Supervision, Funding acquisition.

Declaration of Competing Interest

The authors declare that they have no known competing financial interests or personal relationships that could have appeared to influence the work reported in this paper.

Data availability

Data will be made available on request.

on the supercomputing system in the Supercomputing Center of Wuhan University.

References

Aime, .., Ramos, L., Cipelletti, L., 2018. Microscopic dynamics and failure precursors of a gel under mechanical load. Proc. Natl. Acad. Sci. U. S. A. 115, 3587–3592. https://doi.org/10.1073/pnas.1717403115.

Anantrasirichai, N., Biggs, J., Albino, F., Bull, D., 2019. The Application of Convolutional Neural Networks to Detect Slow, Sustained Deformation in InSAR Time Series. Geophys. Res. Lett. 1–12. 10.1029/2019GL084993.

Bahmani, B., Sun, W., 2022. Manifold embedding data-driven mechanics. J. Mech. Phys. Solids 166, 104927. https://doi.org/10.1016/j.jmps.2022.104927.

Boattini, E., Marín-Aguilar, S., Mitra, S., Foffi, G., Smallenburg, F., Filion, L., 2020. Autonomously revealing hidden local structures in supercooled liquids. Nat. Commun. 11, 1–9. https://doi.org/10.1038/s41467-020-19286-8.

Budrikis, Z., Castellanos, D.F., Sandfeld, S., Zaiser, M., Zapperi, S., 2017. Universal features of amorphous plasticity. Nat. Commun. 8, 1–10. https://doi.org/10.1038/ncomms15928.

Cao, P., Dahmen, K.A., Kushima, A., Wright, W.J., Park, H.S., Short, M.P., Yip, S., 2018a. Nanomechanics of slip avalanches in amorphous plasticity. J. Mech. Phys. Solids 114, 158–171. https://doi.org/10.1016/j.jmps.2018.02.012.

Cao, P., Short, M.P., Yip, S., 2019. Potential energy landscape activations governing plastic flows in glass rheology. Proc. Natl. Acad. Sci. U. S. A. 116, 18790–18797. https://doi.org/10.1073/pnas.1907317116.

Cao, Y., Li, J., Kou, B., Xia, C., Li, Z., Chen, R., Xie, H., Xiao, T., Kob, W., Hong, L., Zhang, J., Wang, Y., 2018b. Structural and topological nature of plasticity in sheared granular materials. Nat. Commun. 9 https://doi.org/10.1038/s41467-018-05329-8.

Cheng, Z., Guo, Z., Tan, Z., Yang, J., Wang, Q., 2019. Waste heat recovery from high-temperature solid granular materials: energy challenges and opportunities. Renew. Sustain. Energy Rev. 116, 109428 https://doi.org/10.1016/j.rser.2019.109428.

Chowdhary, K.R., 2020. Fundamentals of Artificial Intelligence. In: Chowdhary, K.R. (Ed.), Natural Language Processing. Springer India, New Delhi, pp. 603–649. https://doi.org/10.1007/978-81-322-3972-7_19.

Cubuk, E.D., Ivancic, R.J.S., Schoenholz, S.S., Strickland, D.J., Basu, A., Davidson, Z.S., Fontaine, J., Hor, J.L., Huang, Y.-.R., Jiang, Y., Keim, N.C., Koshigan, K.D., Lefever, J.A., Liu, T., Ma, X.-.G., Magagnosc, D.J., Morrow, E., Ortiz, C.P., Rieser, J.M., Shavit, A., Still, T., Xu, Y., Zhang, Y., Nordstrom, K.N., Arratia, P.E., Carpick, R.W., Durian, D.J., Fakhraai, Z., Jerolmack, D.J., Lee, D., Li, J., Riggleman, R., Turner, K.T., Yodh, A.G., Gianola, D.S., Liu, A.J., 2017. Structure-property relationships from universal signatures of plasticity in disordered solids. Science (80-.) 358, 1033–1037. https://doi.org/10.1126/science.aai8830.

Dahmen, K.A., Ben-Zion, Y., Uhl, J.T., 2011. A simple analytic theory for the statistics of avalanches in sheared granular materials. Nat. Phys. 7, 554–557. https://doi.org/10.1038/nphys1957.

Darve, F., Nicot, F., Wautier, A., Liu, J., 2021. Slip lines versus shear bands: two competing localization modes. Mech. Res. Commun. 114 https://doi.org/10.1016/j.mechrescom.2020.103603.

Dauchot, O., Marty, G., Biroli, G., 2005. Dynamical heterogeneity close to the jamming transition in a sheared granular material. Phys. Rev. Lett. 95, 1–4. https://doi.org/10.1103/PhysRevLett.95.265701.

Denisov, D.V., Lörincz, K.A., Uhl, J.T., Dahmen, K.A., Schall, P., 2016. Universality of slip avalanches in flowing granular matter. Nat. Commun. 7 https://doi.org/10.1038/ncomms10641.

Dorostkar, O., Carmeliet, J., 2019. Grain Friction Controls Characteristics of Seismic Cycle in Faults With Granular Gouge. J. Geophys. Res. Solid Earth 124, 6475–6489. https://doi.org/10.1029/2019JB017374.

Dorostkar, O., Carmeliet, J., 2018. Potential Energy as Metric for Understanding Stick–Slip Dynamics in Sheared Granular Fault Gouge: a Coupled CFD–DEM Study. Rock Mech. Rock Eng. 51, 3281–3294. https://doi.org/10.1007/s00603-018-1457-6.

Dorostkar, O., Guyer, R.A., Johnson, P.A., Marone, C., Carmeliet, J., 2017. On the micromechanics of slip events in sheared, fluid-saturated fault gouge. Geophys. Res. Lett. 44, 6101–6108. https://doi.org/10.1002/2017GL073768.

Falk, M.L., Langer, J.S., 1998. Dynamics of viscoplastic deformation in amorphous solids. Phys. Rev. E 57, 7192–7205. https://doi.org/10.1103/PhysRevE.57.7192.

Ferdowsi, B., Griffa, M., Guyer, R.A., Johnson, P.A., Marone, C., Carmeliet, J., 2013. Microslips as precursors of large slip events in the stick-slip dynamics of sheared granular layers: a discrete element model analysis. Geophys. Res. Lett. 40, 4194–4198. https://doi.org/10.1002/grl.50813.

Gao, K., Guyer, R.A., Rougier, E., Johnson, P.A., 2020. Plate motion in sheared granular fault system. Earth Planet. Sci. Lett. 548, 116481 https://doi.org/10.1016/j.epsl.2020.116481.

Ghosh, A., Budrikis, Z., Chikkadi, V., Sellerio, A.L., Zapperi, S., Schall, P., 2017. Direct Observation of Percolation in the Yielding Transition of Colloidal Glasses. Phys. Rev. Lett. https://doi.org/10.1103/PhysRevLett.118.148001.

Guan, S., Qu, T., Feng, Y.T., Ma, G., Zhou, W., 2022. A machine learning-based multi-scale computational framework for granular materials. Acta Geotech. 0123456789. 10.1007/s11440-022-01709-z.

Guo, N., Zhao, J., 2016. 3D multiscale modeling of strain localization in granular media. Comput. Geotech. 80, 360–372. https://doi.org/10.1016/j.compgeo.2016.01.020.

Guo, N., Zhao, J., 2014. A coupled FEM/DEM approach for hierarchical multiscale modelling of granular media. Int. J. Numer. Methods Eng. 99, 789–818. https://doi.org/10.1002/nme.4702.

Hamedmoghadam, H., Jalili, M., Vu, H.L., Stone, L., 2021. Percolation of heterogeneous flows uncovers the bottlenecks of infrastructure networks. Nat. Commun. 12 https://doi.org/10.1038/s41467-021-21483-y.

He, K., Zhang, X., Ren, S., Sun, J., 2016. Deep Residual Learning for Image Recognition. In: Proc. IEEE Conf. Comput. Vis. Pattern Recognit, pp. 770–778. https://doi.org/10.1002/chin.200650130.

Henann, D.L., Kamrin, K., 2014. Continuum thermomechanics of the nonlocal granular rheology. Int. J. Plast. 60, 145–162. https://doi.org/10.1016/j.ijplas.2014.05.002.

Houdoux, D., Amon, A., Marsan, D., Weiss, J., Crassous, J., 2021. Micro-slips in an experimental granular shear band replicate the spatiotemporal characteristics of natural earthquakes. Commun. Earth Environ. 2, 90. https://doi.org/10.1038/s43247-021-00147-1.

Jiang, S.S., Gan, K.F., Huang, Y.J., Xue, P., Ning, Z.L., Sun, J.F., Ngan, A.H.W., 2020. Stochastic deformation and shear transformation zones of the glassy matrix in CuZr-based metallic-glass composites. Int. J. Plast. 125, 52–62. https://doi.org/10.1016/j.ijplas.2019.09.005.

Johnson, P.A., Rouet-Leduc, B., Pyrak-Nolte, L.J., Beroza, G.C., Marone, C.J., Hulbert, C., Howard, A., Singer, P., Gordeev, D., Karaflos, D., Levinson, C.J., Pfeiffer, P., Puk, K.M., Reade, W., 2021. Laboratory earthquake forecasting: a machine learning competition. Proc. Natl. Acad. Sci. U. S. A. 118, 1–10. https://doi.org/10.1073/pnas.2011362118.

Karapiperis, K., Stainier, L., Ortiz, M., Andrade, J.E., 2021. Data-Driven multiscale modeling in mechanics. J. Mech. Phys. Solids 147, 104239. https://doi.org/10.1016/j.jmps.2020.104239.

Karimi, K., Amitrano, D., Weiss, J., 2019. From plastic flow to brittle fracture: role of microscopic friction in amorphous solids. Phys. Rev. E 100. https://doi.org/10.1103/PhysRevE.100.012908.

Kawasaki, T., Araki, T., Tanaka, H., 2007. Correlation between dynamic heterogeneity and medium-range order in two-dimensional glass-forming liquids. Phys. Rev. Lett. 99, 2–5. https://doi.org/10.1103/PhysRevLett.99.215701.

Kim, S., Kamrin, K., 2020. Power-Law Scaling in Granular Rheology across Flow Geometries. Phys. Rev. Lett. 125 https://doi.org/10.1103/PhysRevLett.125.088002.

Kosiba, K., Şopu, D., Scudino, S., Zhang, L., Bednarcik, J., Pauly, S., 2019. Modulating heterogeneity and plasticity in bulk metallic glasses: role of interfaces on shear banding. Int. J. Plast. 119, 156–170. https://doi.org/10.1016/j.ijplas.2019.03.007.

Kou, B., Cao, Y., Li, J., Xia, C., Li, Z., Dong, H., Zhang, A., Zhang, J., Kob, W., Wang, Y., 2018. Translational and Rotational Dynamical Heterogeneities in Granular Systems. Phys. Rev. Lett. 121, 18002. https://doi.org/10.1103/PhysRevLett.121.018002.

Krishnaraj, K.P., Nott, P.R., 2020. Coherent Force Chains in Disordered Granular Materials Emerge from a Percolation of Quasilinear Clusters. Phys. Rev. Lett. 124, 198002 https://doi.org/10.1103/PhysRevLett.124.198002.

Lai, Z., Chen, Q., 2019. Reconstructing granular particles from X-ray computed tomography using the TWS machine learning tool and the level set method. Acta Geotech 14, 1–18. https://doi.org/10.1007/s11440-018-0759-x.

Lherminier, S., Planet, R., Vehel, V.L.D., Simon, G., Vanel, L., Måløy, K.J., Ramos, O., 2019. Continuously Sheared Granular Matter Reproduces in Detail Seismicity Laws. Phys. Rev. Lett. 122 https://doi.org/10.1103/PhysRevLett.122.218501.

Li, L., Homer, E.R., Schuh, C.A., 2013. Shear transformation zone dynamics model for metallic glasses incorporating free volume as a state variable. Acta Mater 61, 3347–3359. https://doi.org/10.1016/j.actamat.2013.02.024.

Liu, H., Xiao, S., Tang, L., Bao, E., Li, E., Yang, C., Zhao, J., Sant, G., Smedskjaer, M.M., Guo, L., Bauchy, M., 2021. Predicting the early-stage creep dynamics of gels from their static structure by machine learning. Acta Mater 210, 22–26. https://doi.org/10.1016/j.actamat.2021.116817.

Liu, J., Nicot, F., Zhou, W., 2018. Sustainability of internal structures during shear band forming in 2D granular materials. Powder Technol 338, 458–470. https://doi.org/10.1016/j.powtec.2018.07.001.

Liu, J., Wautier, A., Bonelli, S., Nicot, F., Darve, F., 2020. Macroscopic softening in granular materials from a mesoscale perspective. Int. J. Solids Struct. 193–194, 222–238. https://doi.org/10.1016/j.ijsolstr.2020.02.022.

Liu, J., Wautier, A., Zhou, W., Nicot, F., Darve, F., 2022. Incremental shear strain chain: a mesoscale concept for slip lines in 2D granular materials. Granul. Matter 24, 1–22. https://doi.org/10.1007/s10035-022-01258-y.

Love, A.E.H., 1927. A Treatise On the Mathematical Theory of Elasticity. Cambridge university press.

Ma, G., Mei, J., Gao, K., Zhao, J., Zhou, W., Wang, D., 2022. Machine learning bridges microslips and slip avalanches of sheared granular gouges. Earth Planet. Sci. Lett. 579, 117366 https://doi.org/10.1016/j.epsl.2022.117366.

Ma, G., Zou, Y., Chen, Y., Tang, L., Ng, Ttat, Zhou, W., 2021. Spatial correlation and temporal evolution of plastic heterogeneity in sheared granular materials. Powder Technol 378, 263–273. https://doi.org/10.1016/j.powtec.2020.09.053.

Ma, G., Zou, Y., Gao, K., Zhao, J., Zhou, W., 2020. Size Polydispersity Tunes Slip Avalanches of Granular Gouge. Geophys. Res. Lett. 47, 1–9. https://doi.org/10.1029/2020 gl090458.

McBeck, J., Aiken, J.M., Ben-Zion, Y., Renard, F., 2020. Predicting the proximity to macroscopic failure using local strain populations from dynamic in situ X-ray tomography triaxial compression experiments on rocks. Earth Planet. Sci. Lett. 543, 116344 https://doi.org/10.1016/j.epsl.2020.116344.

Meier, H.A., Steinmann, P., Kuhl, E., 2008. Towards multiscale computation of confined granular media: contact forces, stresses and tangent operators. Tech. Mech. J. Eng. Mech. 28, 32–42.

Montavon, G., Lapuschkin, S., Binder, A., Samek, W., Müller, K.R., 2017. Explaining nonlinear classification decisions with deep Taylor decomposition. Pattern Recognit 65, 211–222. https://doi.org/10.1016/j.patcog.2016.11.008.

Mungan, M., Sastry, S., Dahmen, K., Regev, I., 2019. Networks and hierarchies: how amorphous materials learn to remember. Phys. Rev. Lett. 123, 178002 https://doi.org/10.1103/PhysRevLett.123.178002.

Murphy, K.A., Dahmen, K.A., Jaeger, H.M., 2019. Transforming Mesoscale Granular Plasticity Through Particle Shape. Phys. Rev. X 9, 11014. https://doi.org/10.1103/PhysRevX.9.011014.

Nicolas, A., Ferrero, E.E., Martens, K., Barrat, J.L., 2018. Deformation and flow of amorphous solids: insights from elastoplastic models. Rev. Mod. Phys. 90, 45006. https://doi.org/10.1103/RevModPhys.90.045006.

Nicot, F., Hadda, N., Guessasma, M., Fortin, J., Millet, O., 2013. On the definition of the stress tensor in granular media. Int. J. Solids Struct. 50, 2508–2517. https://doi.org/10.1016/j.ijsolstr.2013.04.001.

Nicot, F., Sibille, L., Darve, F., 2012. Failure in rate-independent granular materials as a bifurcation toward a dynamic regime. Int. J. Plast. 29, 136–154. https://doi.org/10.1016/j.ijplas.2011.08.002.

Ouadfel, H., Rothenburg, L., 2001. Stress-force-fabric' relationship for assemblies of ellipsoids. Mech. Mater. 33, 201–221. https://doi.org/10.1016/S0167-6636(00)00057-0.

Papadopoulos, L., Porter, M.A., Daniels, K.E., Bassett, D.S., 2018. Network analysis of particles and grains. J. Complex Networks 6, 485–565. https://doi.org/10.1093/COMNET/CNY005.

Paszke, A., Gross, S., Massa, F., Lerer, A., Bradbury, J., Chanan, G., Killeen, T., Lin, Z., Gimelshein, N., Antiga, L., Desmaison, A., Köpf, A., Yang, E., DeVito, Z., Raison, M., Tejani, A., Chilamkurthy, S., Steiner, B., Fang, L., Bai, J., Chintala, S., 2019. PyTorch: an imperative style, high-performance deep learning library. Adv. Neural Inf. Process. Syst. 32, 8024–8035.

Qu, T., Di, S., Feng, Y.T., Wang, M., Zhao, T., 2021. Towards data-driven constitutive modelling for granular materials via micromechanics-informed deep learning. Int. J. Plast. 144, 103046 https://doi.org/10.1016/j.ijplas.2021.103046.

Ramola, K., Chakraborty, B., 2017. Scaling Theory for the Frictionless Unjamming Transition. Phys. Rev. Lett. 118, 1–5. https://doi.org/10.1103/PhysRevLett.118.138001.

Ridout, S., Rocks, J.W., Liu, A.J., 2022. Correlation of plastic events with local structure in jammed packings across spatial dimensions. Proc. Natl. Acad. Sci. U. S. A. 119, 6–11. https://doi.org/10.1073/pnas.2119006119.

Salmenjoki, H., Alava, M.J., Laurson, L., 2018. Machine learning plastic deformation of crystals. Nat. Commun. 9 https://doi.org/10.1038/s41467-018-07737-2.

Shreedharan, S., Bolton, D.C., Rivière, J., Marone, C., 2020. Preseismic Fault Creep and Elastic Wave Amplitude Precursors Scale With Lab Earthquake Magnitude for the Continuum of Tectonic Failure Modes. Geophys. Res. Lett. https://doi.org/10.1029/2020GL086986.

Sun, Y., Gao, Y., Zhu, Q., 2018. Fractional order plasticity modelling of state-dependent behaviour of granular soils without using plastic potential. Int. J. Plast. 102, 53–69. https://doi.org/10.1016/j.ijplas.2017.12.001.

Sundararajan, M., Taly, A., Yan, Q., 2017. Axiomatic attribution for deep networks. arXiv.

Tong, X., Wang, G., Yi, J., Ren, J.L., Pauly, S., Gao, Y.L., Zhai, Q.J., Mattern, N., Dahmen, K.A., Liaw, P.K., Eckert, J., 2016. Shear avalanches in plastic deformation of a metallic glass composite. Int. J. Plast. 77, 141–155. https://doi.org/10.1016/j.ijplas.2015.10.006.

Tordesillas, A., 2007. Force chain buckling, unjamming transitions and shear banding in dense granular assemblies. Philos. Mag. 87, 4987–5016. https://doi.org/10.1080/14786430701594848.

van den Ende, M.P.A., Niemeijer, A.R., 2018. Time-Dependent Compaction as a Mechanism for Regular Stick-Slips. Geophys. Res. Lett. 45, 5959–5967. https://doi.org/10.1029/2018GL078103.

Van Loock, F., Brassart, L., Pardoen, T., 2021. Implementation and calibration of a mesoscale model for amorphous plasticity based on shear transformation dynamics. Int. J. Plast. 145 https://doi.org/10.1016/j.ijplas.2021.103079.

Wang, D., Carmeliet, J., Zhou, W., Dorostkar, O., 2021a. On the Effect of Grain Fragmentation on Frictional Instabilities in Faults With Granular Gouge. J. Geophys. Res. Solid Earth 126. https://doi.org/10.1029/2020JB020510.

Wang, D., Dijksman, J.A., Barés, J., Ren, J., Zheng, H., 2020a. Sheared Amorphous Packings Display Two Separate Particle Transport Mechanisms. Phys. Rev. Lett. 125 https://doi.org/10.1103/PhysRevLett.125.138001.

Wang, K., Sun, W.C., 2018. A multiscale multi-permeability poroplasticity model linked by recursive homogenizations and deep learning. Comput. Methods Appl. Mech. Eng. 334, 337–380. https://doi.org/10.1016/j.cma.2018.01.036.

Wang, Q., Jain, A., 2019. A transferable machine-learning framework linking interstice distribution and plastic heterogeneity in metallic glasses. Nat. Commun. 10, 1–11. https://doi.org/10.1038/s41467-019-13511-9.

Wang, X., Zhang, H., Douglas, J.F., 2021b. The initiation of shear band formation in deformed metallic glasses from soft localized domains. J. Chem. Phys. 155 https://doi.org/10.1063/5.0069729.

Wang, Y., Wang, Yujie, Zhang, J., 2020b. Connecting shear localization with the long-range correlated polarized stress fields in granular materials. Nat. Commun. https://doi.org/10.1038/s41467-020-18217-x.

Wautier, A., Bonelli, S., Nicot, F., 2019. Rattlers' contribution to granular plasticity and mechanical stability. Int. J. Plast. 112, 172–193. https://doi.org/10.1016/j.ijplas.2018.08.012.

Wautier, A., Bonelli, S., Nicot, F., 2018. Micro-inertia origin of instabilities in granular materials. Int. J. Numer. Anal. Methods Geomech. 42, 1037–1056. https://doi.org/10.1002/nag.2777.

Wu, Y., Bei, H., Wang, Y.L., Lu, Z.P., George, E.P., Gao, Y.F., 2015. Deformation-induced spatiotemporal fluctuation, evolution and localization of strain fields in a bulk metallic glass. Int. J. Plast. 71, 136–145. https://doi.org/10.1016/j.ijplas.2015.05.006.

Xia, C., Li, J., Cao, Y., Kou, B., Xiao, X., Fezzaa, K., Xiao, T., Wang, Y., 2015. The structural origin of the hard-sphere glass transition in granular packing. Nat. Commun. 6, 1–9. https://doi.org/10.1038/ncomms9409.

Xiong, H., Nicot, F., Yin, Z.Y., 2017. A three-dimensional micromechanically based model. Int. J. Numer. Anal. Methods Geomech. 41, 1669–1686. https://doi.org/10.1002/nag.2692.

Zhai, C., Albayrak, N., Engqvist, J., Hall, S.A., Wright, J., Majkut, M., Herbold, E.B., Hurley, R.C., 2022. Quantifying local rearrangements in three-dimensional granular materials: rearrangement measures, correlations, and relationship to stresses. Phys. Rev. E 105, 1–17. https://doi.org/10.1103/physreve.105.014904.

Zhang, G., Ridout, S., Liu, A.J., 2020. Interplay of rearrangements, strain, and local structure during avalanche propagation. Phys. Rev. X 11, 41019. https://doi.org/10.1103/PhysRevX.11.041019.

Zheng, J., Sun, A., Wang, Y., Zhang, J., 2018. Energy Fluctuations in Slowly Sheared Granular Materials. Phys. Rev. Lett. 121 https://doi.org/10.1103/PhysRevLett.121.248001.

Zheng, J., Xing, Y., Yuan, Y., Li, Z., Zeng, Z., Zhang, S., Yuan, H., Tong, H., Xia, C., Kob, W., Jia, X., Zhang, J., Wang, Y., 2021. Influence of Roughness on Granular Avalanches. arXiv.

Zhou, S., Tordesillas, A., Pouragha, M., Bailey, J., Bondell, H., 2021. On local intrinsic dimensionality of deformation in complex materials. Sci. Rep. 11, 1–14. https://doi.org/10.1038/s41598-021-89328-8.

Zhu, H., Nguyen, H.N.G., Nicot, F., Darve, F., 2016a. On a common critical state in localized and diffuse failure modes. J. Mech. Phys. Solids 95, 112–131. https://doi.org/10.1016/j.jmps.2016.05.026.

Zhu, H., Nicot, F., Darve, F., 2016b. Meso-structure organization in two-dimensional granular materials along biaxial loading path. Int. J. Solids Struct. 96, 25–37. https://doi.org/10.1016/j.ijsolstr.2016.06.025.